Supporting Information

Patrick et al. 10.1073/pnas.1319000111

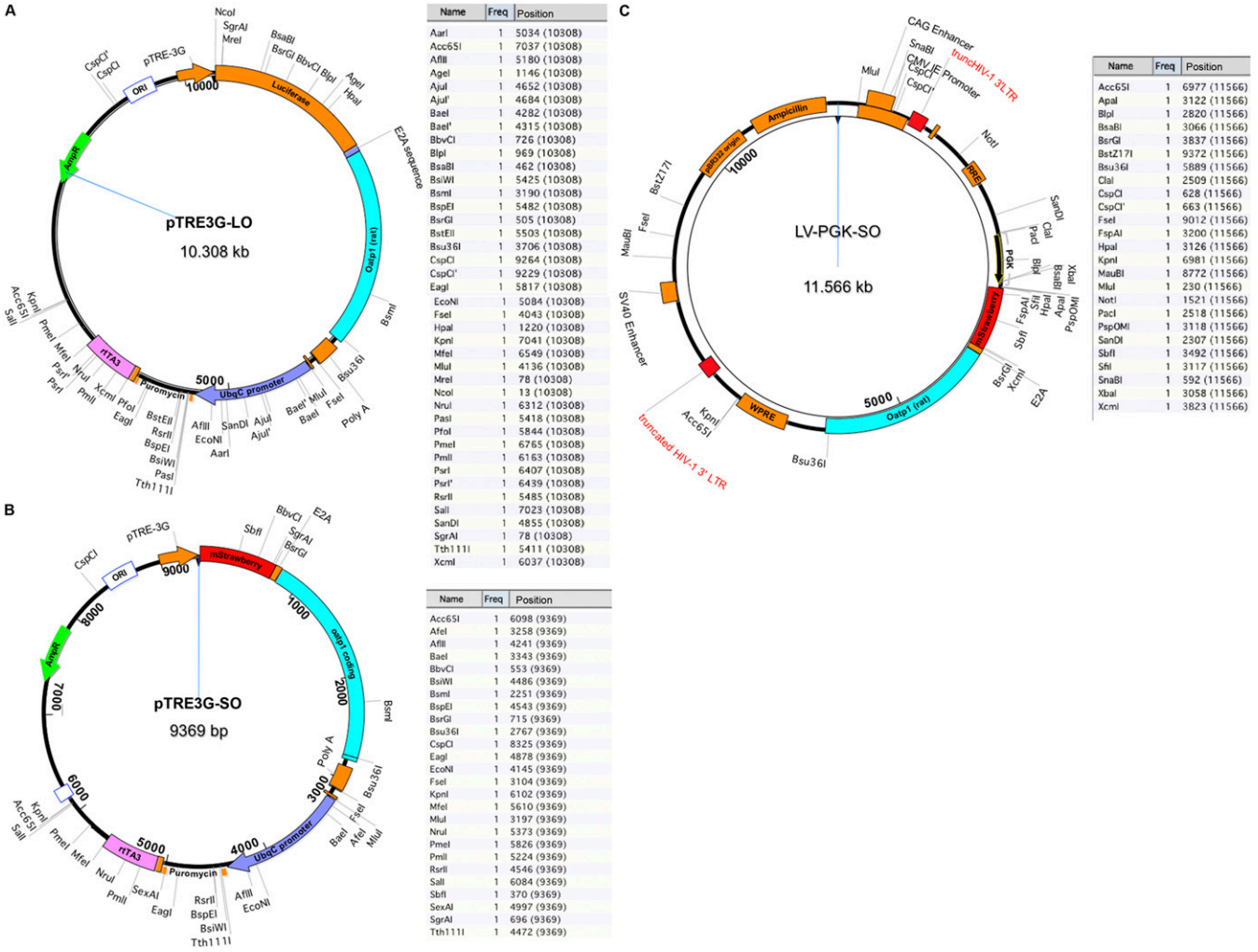

Name	Freq	Position
AarI	1	5034 (10308)
Acc65I	1	7037 (10308)
AflII	1	5180 (10308)
AgeI	1	1146 (10308)
AjuI	1	4652 (10308)
AjuI'	1	4684 (10308)
BaeI	1	4282 (10308)
BaeI'	1	4315 (10308)
BbvCI	1	726 (10308)
BlpI	1	969 (10308)
BsaBI	1	462 (10308)
BsiWI	1	5425 (10308)
BsmI	1	3190 (10308)
BspEI	1	5482 (10308)
BsrGI	1	505 (10308)
BstEII	1	5503 (10308)
Bsu36I	1	3706 (10308)
CspCI	1	9264 (10308)
CspCI'	1	9229 (10308)
EagI	1	5817 (10308)
EcoNI	1	5084 (10308)
FseI	1	4043 (10308)
HpaI	1	1220 (10308)
KpnI	1	7041 (10308)
MfeI	1	6549 (10308)
MluI	1	4136 (10308)
MreI	1	78 (10308)
NcoI	1	13 (10308)
NruI	1	6312 (10308)
PasI	1	5418 (10308)
PfoI	1	5844 (10308)
PmeI	1	6765 (10308)
PmlI	1	6163 (10308)
PsrI	1	6407 (10308)
PsrI'	1	6439 (10308)
RsrII	1	5485 (10308)
SalI	1	7023 (10308)
SanDI	1	4855 (10308)
SgrAI	1	78 (10308)
Tth111I	1	5411 (10308)
XcmI	1	6037 (10308)

Name	Freq	Position
Acc65I	1	6098 (9369)
AfeI	1	3258 (9369)
AflII	1	4241 (9369)
BaeI	1	3343 (9369)
BbvCI	1	553 (9369)
BsiWI	1	4486 (9369)
BsmI	1	2251 (9369)
BspEI	1	4543 (9369)
BsrGI	1	715 (9369)
Bsu36I	1	2767 (9369)
CspCI	1	8325 (9369)
EagI	1	4878 (9369)
EcoNI	1	4145 (9369)
FseI	1	3104 (9369)
KpnI	1	6102 (9369)
MfeI	1	5610 (9369)
MluI	1	3197 (9369)
NruI	1	5373 (9369)
PmeI	1	5826 (9369)
PmlI	1	5224 (9369)
RsrII	1	4546 (9369)
SalI	1	6084 (9369)
SbfI	1	370 (9369)
SexAI	1	4997 (9369)
SgrAI	1	696 (9369)
Tth111I	1	4472 (9369)

Name	Freq	Position
Acc65I	1	6977 (11566)
ApaI	1	3122 (11566)
BlpI	1	2820 (11566)
BsaBI	1	3066 (11566)
BsrGI	1	3837 (11566)
BstZ17I	1	9372 (11566)
Bsu36I	1	5889 (11566)
ClaI	1	2509 (11566)
CspCI	1	628 (11566)
CspCI'	1	663 (11566)
FseI	1	9012 (11566)
FspAI	1	3200 (11566)
HpaI	1	3126 (11566)
KpnI	1	6981 (11566)
MauBI	1	8772 (11566)
MluI	1	230 (11566)
NotI	1	1521 (11566)
PacI	1	2518 (11566)
PspOMI	1	3118 (11566)
SanDI	1	2307 (11566)
SbfI	1	3492 (11566)
SfiI	1	3117 (11566)
SnaBI	1	592 (11566)
XbaI	1	3058 (11566)
XcmI	1	3823 (11566)

Fig. S1. Plasmid maps for the vectors used in this study. (*A*) Doxycycline-inducible luciferase–E2A–Oatp1. (*B*) Doxycycline-inducible mStrawberry–E2A–Oatp1. (*C*) Lentiviral-packaging plasmid pBOBI with constitutive PGK (phosphoglycerate kinase) promoter and mStrawberry–E2A–Oatp1 coding sequence.

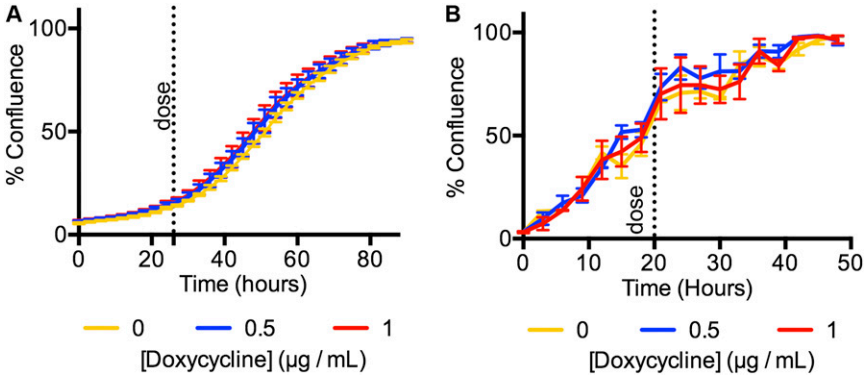

Fig. S2. Viability was not reduced by Oatp1 expression. (*A*) Clonal HEK 293T and (*B*) HCT 116 cells carrying the luciferase–E2A–Oatp1 transgene, regulated by a TRE3G doxycycline-inducible promoter, were induced at the indicated time (vertical dotted line) with the indicated concentration of doxycycline. Growth was assessed by measuring the degree of confluence on the plate (Incucyte, Essen Bioscience), with three replicate wells read per condition and nine fields of view per well. Error bars show SEM.

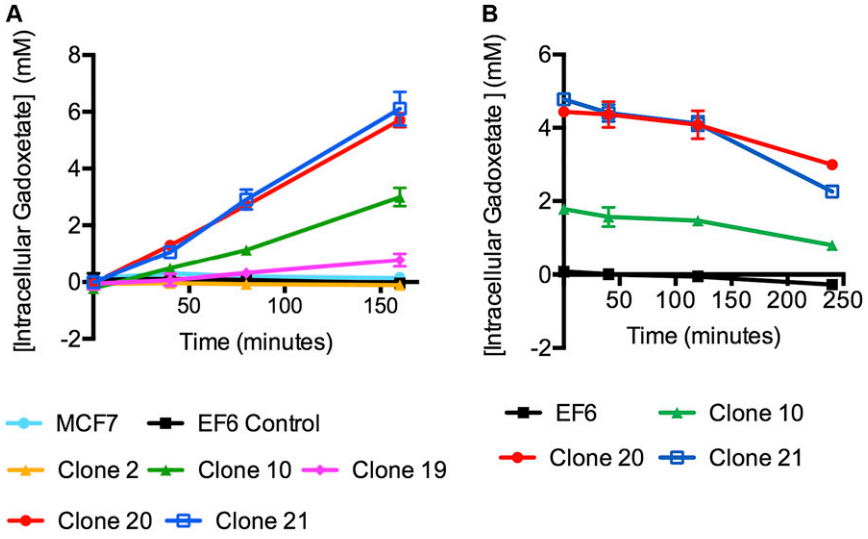

Fig. S3. Gadolinium-ethoxybenzyl-diethylenetriamine pentaacetic acid (Gd-EOB-DTPA) uptake and washout in MCF-7 cells transfected to express Oatp1. Measurements of uptake (*A*) and washout (*B*) in untransfected MCF-7 cells, in MCF-7 cells stably transfected with the empty vector (EF6) and in MCF-7 cells stably transfected with a vector expressing Oatp1a1. For uptake measurements, cells were incubated with 5 mM Gd-EOB-DTPA for the indicated times in transport buffer at 37 °C. For the efflux measurements, cells were preloaded by incubation with 5 mM Gd-EOB-DTPA for 120 min. They were then washed twice with ice-cold transport buffer and incubated in this buffer at 37 °C. The Gd^{3+}-chelate concentration was measured in cell lysates using an inversion recovery T_1 measurement and assuming a molar relaxivity for the chelate of 5.7 $mM^{-1}{\cdot}s^{-1}$. The intracellular concentration was calculated by assuming that 120 mg of protein corresponds to 0.64 mL intracellular water (1). The points represent the average of three independent experiments (with each sample measured in triplicate) for uptake and two independent experiments for washout.

1. Reitzer LJ, Wice BM, Kennell D (1979) Evidence that glutamine, not sugar, is the major energy source for cultured HeLa cells. *J Biol Chem* 254(8):2669–2676.

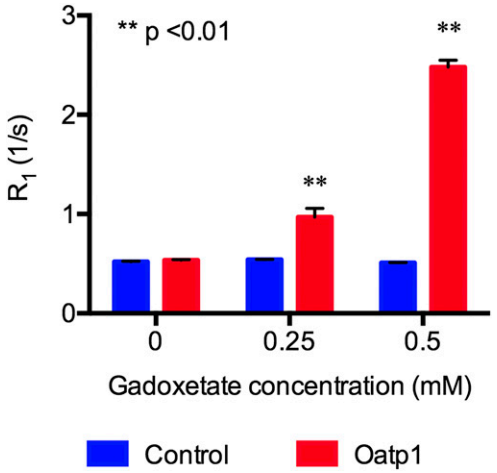

Fig. S4. Gd-EOB-DTPA uptake in HEK 293T cells expressing Oatp1. Relaxation rates ($R_1 = 1/T_1$) were measured by T_1 imaging of washed pellets of HEK 293T cells that had been incubated for 90 min with 0.0, 0.25 or 0.5 mM Gd-EOB-DTPA. Both cell lines (control and Oatp1) expressed luciferase–YFP. The Oatp1 cells also expressed mStrawberry–Oatp1. R_1 was significantly increased in cells expressing Oatp1 compared with control cells (**$P < 0.01$, two-tailed unpaired t test, $n = 3$). Error bars show SEM.

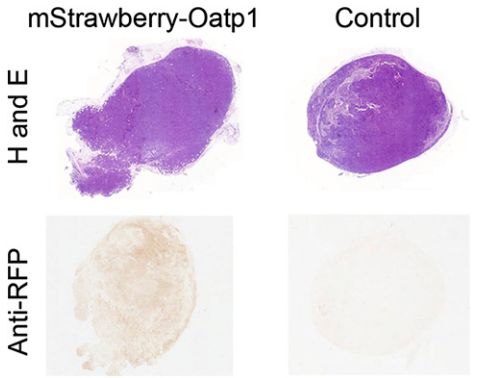

Fig. S5. HEK 293T xenograft histology. Xenografts from a representative mouse were excised 80 h after Gd-EOB-DTPA administration (Fig. 4), fixed for 24 h in paraformaldehyde, paraffin-embedded, and sectioned. Hematoxylin/eosin (H&E) staining showed minimal necrosis in both xenografts. Immunohistochemical staining for the red fluorescent protein (RFP) mStrawberry confirmed expression of the mStrawberry–Oatp1 transgene.

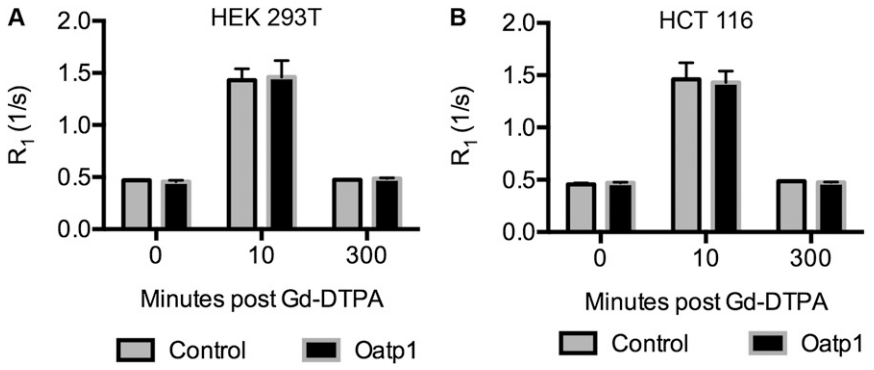

Fig. S6. Gd-DTPA shows similar enhancement in muscle and control xenografts and xenografts expressing Oatp1. Gd-DTPA was injected at 0.664 mmoles/kg, following washout of Gd-EOB-DTPA (Fig. 4). Bars represent R_1 of control and Oatp1-expressing xenografts at the indicated times postinjection. There was no significant difference in R_1 between control xenografts and xenografts expressing Oatp1 at 10 min or 5 h after contrast agent injection (two-tailed t test, $n = 2$), for either (*A*) HEK 293T xenografts or (*B*) HCT 116 xenografts. Error bars show SEM.

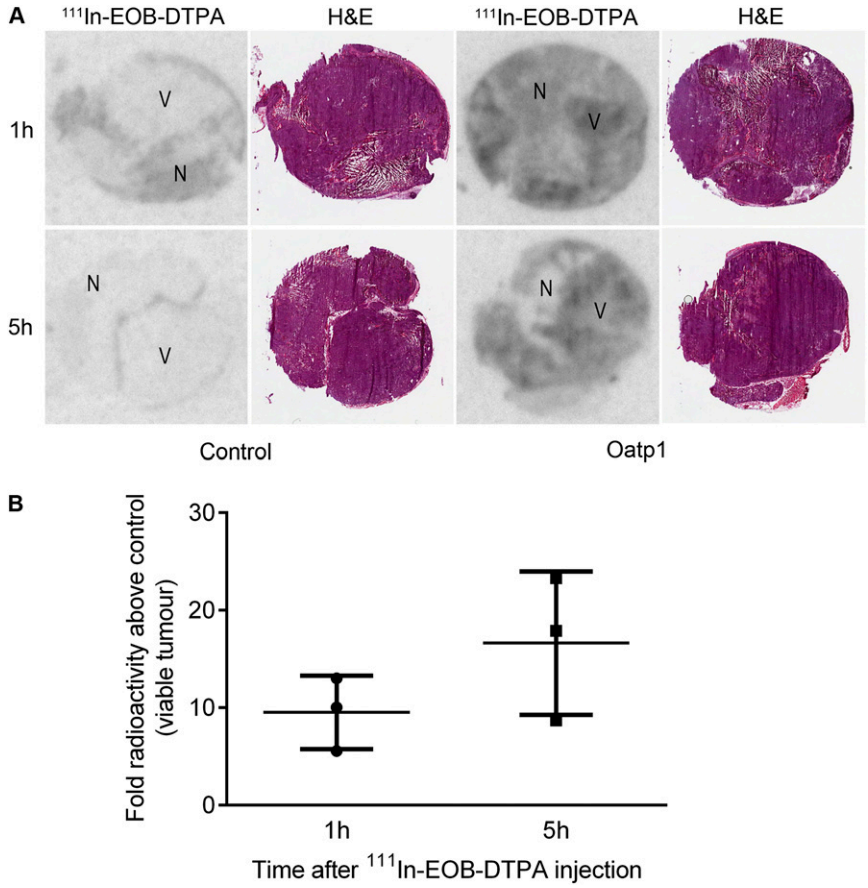

Fig. S7. Autoradiography showed a correlation between ^{111}In-EOB-DTPA uptake and tissue viability in Oatp1-expressing xenografts. (*A*) Representative autoradiograms and the corresponding H&E-stained sections from HEK 293T xenografts. The H&E-stained sections showed the viable (V) and necrotic (N) regions of the xenografts. Control xenografts accumulated ^{111}In-EOB-DTPA in necrotic regions at 1 h after injection, which had cleared by 5 h. Xenografts expressing Oatp1 accumulated ^{111}In-EOB-DTPA in viable tissue, and to a lesser extent in necrotic regions at 1 h after injection, but this had cleared from the necrotic regions by 5 h, leaving signals largely in the viable regions of the xenografts. (*B*) The ratio of background-corrected activity in viable regions of xenografts expressing Oatp1 versus viable regions of control xenografts ($n = 3$). Viable and necrotic regions were determined from the corresponding H&E-stained sections. The error bars show the mean and SD.

Table S1. Magnetic resonance gene reporters described previously

Gene reporter	Substrate	Contrast type	Fold contrast	Promoter	Vector	Tissue type	Refs.
Creatine kinase	Phosphocreatine (endogenous and supplemented)	^{31}P NMR	Twenty-threefold increase in phosphocreatine/ATP ratio compared with control	Transthyretin (liver -specific promotor)	Plasmid used to transfect pronuclei (transgenic mice)	Liver	(1)
	Phosphocreatine (endogenous and supplemented)	^{31}P NMR	Not stated	CMV	Adenovirus via tail vein injection	Liver	(2)
Tyrosinase	Endogenous iron	T_2	1.35-fold in vivo	CMV	Plasmid	Mouse fibroblasts, HEK 293T	(3)
	Endogenous iron	T_2/T_1	T_2 - 36%, T_1 - 26%, enhancement in vivo	CMV	Plasmid	MCF-7 xenograft	(4)
Transferrin receptor	Tf-MIONs	T_2	5.3-fold decrease in signal in vivo	hTR	Plasmid	9L gliosarcoma	(5)
	Tf-MIONs	T_2/T_1	2.4-fold decrease in T_2, 1.28-fold enhancement of T_1, in vivo	Tet-off	Plasmid	9L gliosarcoma	(6)
LacZ	EGadMe (LacZ cleavable Gd^{3+} -based contrast agent)	T_1	T_1 57% enhancement in vivo	N/A	mRNA	*Xenopus* embryonic tissue	(7)
	OFPNPG (2-Fluoro-4-nitrophenol -beta-D-galactopyranoside)	^{19}F	Not stated, only performed in vitro	CMV	Plasmid	MCF-7, 9L glioma	(8)
	OFPNPG	^{19}F	Signal-to-noise ratio of 20–30 in ^{19}F spectra (after direct injection into tumor)	CMV	Plasmid	PC3 prostate tumor	(9)
	S-Gal, and ^{19}F S-gal	^{19}F/T_2	36% increase in R_2, (intratumoral injection) ^{19}F did not work in vivo	CMV	Plasmid	PC3 prostate tumor	(10)
	S-Gal	T_2	3.5-fold decrease in signal compared with control after injection (intratumoral)	CMV	Plasmid	MCF-7	(11)
Arginine kinase	Endogenous arginine	^{31}P NMR	Phosphoarginine concentration comparable to that of phosphocreatine	CMV	Adenovirus	Skeletal muscle	(12)
Ferritin	Endogenous iron	T_2	12% increase in R_2 in vivo	Tet-off	Plasmid	C6 glioma	(13)
	Endogenous iron	T_2	2.5-fold increase in R_2 in vitro, not stated for in vivo	CMV	Adenovirus	Mouse brain	(14)
Ferritin and transferrin receptor	Supplementary iron	T_2	21% R_2* enhancement ex vivo	Sv40	Electroporation with pZeoSV2 plasmid	C17 glioma	(15)
BAP-TM	Bis-5-HT-DTPA(Gd)/streptavidin-MNP/streptavidin–Alexa 680	T_1/T_2	twofold increase in R_2, 3.3-fold increase in R_1 ($n = 1$)	CMV	Lentivirus	BHK12	(16)
VTC/VMA 2	Endogenous	^{31}P NMR	Not stated	Gal1	Plasmid	*Saccharomyces cerevisiae*	(17)
Lysine-rich protein	N/A	CEST	8.2% enhancement vs. 3.5% for control	CMV	pIRES2-EGFP, stable transfection with plasmid	9L glioma	(18)
MagA	Iron supplement	T_2	Three- to fourfold change in R_2 in vitro, not stated for in vivo	CMV/Tet CMV	Lentivirus	293FT	(19)
Carboxypeptidase G2	Hyperpolarized 3,5-DFBGlu	^{13}C NMR	Not stated	N/A	N/A	N/A (experiments done in solution)	(20)
Aminoacylase	Hyperpolarized [1-^{13}C]*N*-acetyl-L-methionine	^{13}C NMR	Not stated for in vitro, signal-to-noise ratio of 17 in solution	CMV	pcDNA 3.1	HEK 293T in vitro	(21)

Table S1. Cont.

Gene reporter	Substrate	Contrast type	Fold contrast	Promoter	Vector	Tissue type	Refs.
mbGlucBiotin	^{111}In-DTPA-biotin, coelenterazine, magnetic nanoparticles	T_2, PET, bioluminescence	Twofold increase in R_2 in vivo	CMV	Lentivirus (polyclonal cells)	Gli36 glioma cells	(22)
DMT1	Manganese chloride	T_1	1.6 to 1.8-fold R_1 enhancement in vivo	CAG	Plasmid/lentiviral	HEK, B16, GL26, neonate mouse brain	(23)
HSV-TK	5-methyl-5,6-dihydrothymidine	CEST	Change of 2% in signal	CMV	Lentivirus	9L glioma	(24)

CAG, cytomegalovirus-β-actin-β-globin; CEST, chemical exchange saturation transfer; DMT1, divalent metal ion transporter; MIONs, monocrystalline iron oxide nanoparticles; MNPs, magnetic nanoparticles; N/A, not applicable; PET, positron emission tomography.
*Measurement of a specific type of relaxation that differs from R2.

1. Koretsky AP, Brosnan MJ, Chen LH, Chen JD, Van Dyke T (1990) NMR detection of creatine kinase expressed in liver of transgenic mice: Determination of free ADP levels. *Proc Natl Acad Sci USA* 87(8):3112–3116.
2. Auricchio A, Zhou R, Wilson JM, Glickson JD (2001) In vivo detection of gene expression in liver by ^{31}P nuclear magnetic resonance spectroscopy employing creatine kinase as a marker gene. *Proc Natl Acad Sci USA* 98(9):5205–5210.
3. Weissleder R, et al. (1997) MR imaging and scintigraphy of gene expression through melanin induction. *Radiology* 204(2):425–429.
4. Alfke H, et al. (2003) In vitro MR imaging of regulated gene expression. *Radiology* 228(2):488–492.
5. Weissleder R, et al. (2000) In vivo magnetic resonance imaging of transgene expression. *Nat Med* 6(3):351–355.
6. Moore A, Josephson L, Bhorade RM, Basilion JP, Weissleder R (2001) Human transferrin receptor gene as a marker gene for MR imaging. *Radiology* 221(1):244–250.
7. Louie AY, et al. (2000) In vivo visualization of gene expression using magnetic resonance imaging. *Nat Biotechnol* 18(3):321–325.
8. Kodibagkar VD, Yu J, Liu L, Hetherington HP, Mason RP (2006) Imaging beta-galactosidase activity using 19F chemical shift imaging of LacZ gene-reporter molecule 2-fluoro-4-nitrophenol-beta-D-galactopyranoside. *Magn Reson Imaging* 24(7): 959–962.
9. Liu L, Kodibagkar VD, Yu JX, Mason RP (2007) ^{19}F-NMR detection of lacZ gene expression via the enzymic hydrolysis of 2-fluoro-4-nitrophenyl beta-D-galactopyranoside in vivo in PC3 prostate tumor xenografts in the mouse. *FASEB J* 21(9):2014–2019.
10. Yu JX, Kodibagkar VD, Hallac RR, Liu L, Mason RP (2012) Dual 19F/1H MR gene reporter molecules for in vivo detection of β-galactosidase. *Bioconjug Chem* 23(3):596–603.
11. Cui W, Liu L, Kodibagkar VD, Mason RP (2010) S-Gal, a novel ^{1}H MRI reporter for beta-galactosidase. *Magn Reson Med* 64(1):65–71.
12. Walter G, Barton ER, Sweeney HL (2000) Noninvasive measurement of gene expression in skeletal muscle. *Proc Natl Acad Sci USA* 97(10):5151–5155.
13. Cohen B, Dafni H, Meir G, Harmelin A, Neeman M (2005) Ferritin as an endogenous MRI reporter for noninvasive imaging of gene expression in C6 glioma tumors. *Neoplasia* 7(2):109–117.
14. Genove G, DeMarco U, Xu H, Goins WF, Ahrens ET (2005) A new transgene reporter for in vivo magnetic resonance imaging. *Nat Med* 11(4):450–454.
15. Deans AE, et al. (2006) Cellular MRI contrast via coexpression of transferrin receptor and ferritin. *Magn Reson Med* 56(1):51–59.
16. Tannous BA, et al. (2006) Metabolic biotinylation of cell surface receptors for in vivo imaging. *Nat Methods* 3(5):391–396.
17. Ki S, et al. (2006) A novel magnetic resonance-based method to measure gene expression in living cells. *Nucleic Acids Res* 34(6):e51.
18. Gilad AA, et al. (2007) Artificial reporter gene providing MRI contrast based on proton exchange. *Nat Biotechnol* 25(2):217–219.
19. Zurkiya O, Chan AW, Hu X (2008) MagA is sufficient for producing magnetic nanoparticles in mammalian cells, making it an MRI reporter. *Magn Reson Med* 59(6):1225–1231.
20. Jamin Y, et al. (2009) Hyperpolarized (13)C magnetic resonance detection of carboxypeptidase G2 activity. *Magn Reson Med* 62(5):1300–1304.
21. Chen AP, Hurd RE, Gu YP, Wilson DM, Cunningham CH (2011) (13)C MR reporter probe system using dynamic nuclear polarization. *NMR Biomed* 24(5):514–520.
22. Niers JM, et al. (2012) Single reporter for targeted multimodal in vivo imaging. *J Am Chem Soc* 134(11):5149–5156.
23. Bartelle BB, Szulc KU, Suero-Abreu GA, Rodriguez JJ, Turnbull DH (2013) Divalent metal transporter, DMT1: A novel MRI reporter protein. *Magn Reson Med* 70(3):842–850.
24. Bar-Shir A, et al. (2013) Transforming thymidine into a magnetic resonance imaging probe for monitoring gene expression. *J Am Chem Soc* 135(4):1617–1624.

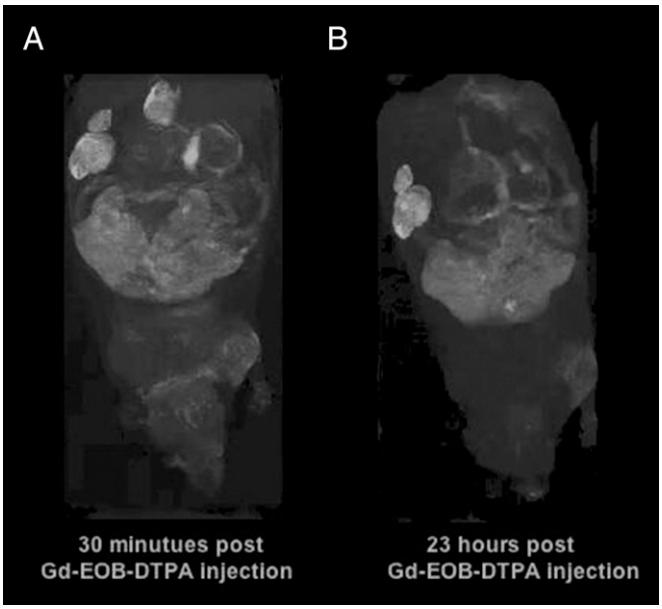

Movie S1. Three-dimensional gradient-echo pulse sequence taken 30–60 min (*Left*) and 23 h (*Right*) after injection of 0.664 mmoles/kg Gd-EOB-DTPA, from a representative mouse bearing Oatp1-expressing (right flank) and control (left flank) xenografts. Oatp1-expressing xenograft appears hyperintense. Enhancement is also visible in the liver.

Movie S1